Rotational Magnetic Moments of Alkali-Halide Molecules

F. MEHRAN, R. A. BROOKS, AND N. F. RAMSEY
Lyman Laboratory, Harvard University, Cambridge, Massachusetts
(Received 29 July 1965)

The rotational magnetic moments of a number of alkali-halide molecules have been measured by the molecular-beam magnetic-resonance technique. The gyromagnetic ratios in units of nuclear magnetons are:

Li^7F^{19}	(+)0.07367±0.00050	$K^{39}F^{19}$	(−)0.0364±0.0012
Li^7Cl^{35}	(+)0.0848±0.0032	$Rb^{85}F^{19}$	(−)0.0441±0.0028
Li^6Cl^{35}	(+)0.1042±0.0033	$Rb^{85}Cl^{35}$	(−)0.0183±0.0018
Li^7Br	(+)0.0911±0.0089	$Cs^{133}F^{19}$	(−)0.0621±0.0055
$Na^{23}I^{127}$	(+)0.0268±0.0047	$Cs^{133}Cl^{35}$	(−)0.0212±0.0011.

Only the absolute values were determined experimentally. However, the absolute values are reasonably consistent with the theoretical ones, so signs from the theory are listed above in parentheses. It is shown that for weak fields the molecular rotational magnetic moments do not correspond directly to the peaks of the reasonance curves. A statistical analysis has been carried out to determine the rotational g values from the peaks of the observed resonances. Since the correction is large (up to 50%), the above results would be wrong by an amount beyond the indicated experimental error if the interpretation of the correction is not valid. No such uncertainty arises in the LiF measurements or in other rotational-moment measurements where the correction does not need to be made. The measured values determined in accordance with the above analysis are found to be in good agreement with the predictions from a theory of Foley. The spin-rotational interaction constant of F^{19} in $Cs^{133}F^{19}$ has been measured by a new method to be 13.5±2.5 kc/sec.

I. INTRODUCTION

THE rotational gyromagnetic ratios of most diatomic molecules are so small that their measurements by the molecular-beam magnetic-resonance method were originally believed to be impossible. If only single quantum transitions occur in the radiofrequency (rf) region, the deflections that the molecules undergo at the detector will be so small that the transitions will not be observable. What was, until recently, overlooked in rotational magnetic moment measurements was the possibility of using multiple quantum transitions. At high source temperatures the most probable angular momenta of these molecules are so large that the rotational magnetic moments are of the same order of magnitude as the nuclear magnetic moments, despite the small gyromagnetic ratios. Therefore, if the angular momentum is rotated through a large angle about an axis perpendicular to the quantization axis, the change in the component of the angular momentum along the quantization axis will be sufficiently large to be easily detectable, as discussed by Lawrence *et al.*, and Pinkerton,[1] Cederberg *et al.*,[2] and Brooks *et al.*[3]

If the energy levels are equally spaced, and if the molecule is still in the radiofrequency region after it has made its first transition, the molecule will undergo a second transition. If we give the molecule enough time in the rf region, it will make many transitions. Classically, this can be pictured as a reversal of the direction of the angular momentum by rotation about an axis perpendicular to the axis of the external magnetic field. One way to cause the angular momentum to undergo a large rotation is to increase the rate of rotation of the angular momentum by increasing the rf field.

The theory of multiple quantum transitions and the formulas for optimum transitions have been worked out by Pinkerton,[1] and by Cederberg and Ramsey.[2]

The first rotational moments measured by the multiple transition technique were those of the molecules which had no internal interactions.[2] Subsequently, several molecules were studied which had nonzero but small interactions, so that a strong field approximation was applicable.[3] In the case of most of the alkali-halide molecules, the quadrupole interaction energy of at least one nucleus is so large that the strong field approximation is impossible with any attainable external field. The angular momentum of at least one nucleus remains coupled to the rotational angular momentum. As a result, in such cases the peak of the observed resonance does not correspond to the rotational g factor.

As is shown in the following sections, the peak of the resonance curve corresponds to a g factor which is a combination of the rotational g factor and a function of the nuclear g factor. An analysis has been carried out to determine the rotational g factor from the peak of the observed resonance.

The molecular-beam machine used in our experiments is the one built by Kolsky, Phipps, Ramsey, and Silsbee[4] and modified by others.[5,6] The various features of the machine have recently been described.[3]

[1] T. R. Lawrence, C. H. Anderson, and N. F. Ramsey, Phys. Rev. **130**, 1865 (1963); J. N. Pinkerton, Ph.D. thesis, Harvard University, 1961 (unpublished).
[2] J. W. Cederberg and N. F. Ramsey, Phys Rev. **135**, A39 (1964).
[3] R. A. Brooks, C. H. Anderson, and N. F. Ramsey, Phys. Rev. **136**, A62 (1964).
[4] H. G. Kolsky, T. E. Phipps, N. F. Ramsey, and H. B. Silsbee, Phys. Rev. **87**, 395 (1952).
[5] W. E. Quinn, A. Pery, J. M. Baker, H. R. Lewis, N. F. Ramsey, and J. T. LaTourrette, Rev. Sci. Instr. **29**, 935 (1958).
[6] R. J. Kolenkow, Ph.D. thesis, Harvard University, 1959 (unpublished); T. R. Lawrence, Ph.D. thesis, Harvard University, 1961 (unpublished).

II. STATISTICAL ANALYSIS

1. The Hamiltonian

The orientation-dependent part of the Hamiltonian for a $^1\Sigma$ heteronuclear diatomic molecule in an external magnetic field is[7]

$$H=-[1-\sigma_1(J)]g_1\mu_N\mathbf{I}_1\cdot\mathbf{H}-[1-\sigma_2(J)]g_2\mu_N\mathbf{I}_2\cdot\mathbf{H}-g_J\mu_N\mathbf{J}\cdot\mathbf{H}-c_1h\mathbf{I}_1\cdot\mathbf{J}-c_2h\mathbf{I}_2\cdot\mathbf{J}$$
$$-\frac{(eqQ)_1}{2I_1(2I_1-1)(2J+3)(2J-1)}[3(\mathbf{I}_1\cdot\mathbf{J})^2+\tfrac{3}{2}(\mathbf{I}_1\cdot\mathbf{J})-\mathbf{I}_1^2\mathbf{J}^2]$$
$$-\frac{(eqQ)_2}{2I_2(2I_2-1)(2J+3)(2J-1)}[3(\mathbf{I}_2\cdot\mathbf{J})^2+\tfrac{3}{2}(\mathbf{I}_2\cdot\mathbf{J})-\mathbf{I}_2^2\mathbf{J}^2]. \quad (1)$$

Both the direct and the electron coupled nuclear spin-spin interactions and the diamagnetic interaction are omitted since they are negligible to the present accuracy for alkali-halide molecules.

I_1, I_2, and J are "good" quantum numbers throughout our discussions. Therefore, the substitutions

$$\mathbf{I}_1^2=I_1(I_1+1),\quad \mathbf{I}_2^2=I_2(I_2+1),$$

and

$$\mathbf{J}^2=J(J+1)$$

in Eq. (1) will be made.

J is a large quantum number. The most probable values of J for our molecules range between 20 and 70.

J_m, the most probable J, is

$$J_m=(kTI)^{1/2}/\hbar. \quad (2)$$

This value of J maximizes the Boltzmann distribution function

$$P(J)=(\hbar/kTI)Je-(J^2\hbar^2/2kTI). \quad (3)$$

Because J is large, we can approximate $J(J+1)$ by J^2 and $(2J+3)(2J-1)$ by $4J^2$ in Eq. (1). The factors σ and c_{alkali} are negligible.

Making the above adjustments and omitting the negligible terms, Eq. (1) will read

$$H=-g_1\mu_N\mathbf{I}_1\cdot\mathbf{H}-g_2\mu_N\mathbf{I}_2\cdot\mathbf{H}-g_J\mu_N\mathbf{J}\cdot\mathbf{H}-c_Hh\mathbf{I}_H\cdot\mathbf{J}-((eqQ)_1/8I_1(2I_1-1)J^2)[3(\mathbf{I}_1\cdot\mathbf{J})^2+\tfrac{3}{2}(\mathbf{I}_1\cdot\mathbf{J})-I_1(I_1+1)J^2]$$
$$-((eqQ)_2/8I_2(2I_2-1)J^2)[3(\mathbf{I}_2\cdot\mathbf{J})^2+\tfrac{3}{2}(\mathbf{I}_2\cdot\mathbf{J})-I_2(I_2+1)J^2], \quad (4)$$

where c_H is the spin-rotation constant of the halide nucleus.

2. The Choice of Representation

In order to obtain the energy levels from Eq. (4), a suitable representation must be chosen. Depending on the relative strengths of the internal interactions and the interactions with the external field, four cases arise:

(a) Both nuclei primarily coupled to the external field (strong field approximation).

In this case, the external field is so large that both $\mathbf{I}_1$ and $\mathbf{I}_2$ are decoupled from $\mathbf{J}$ and $\mathbf{I}_1$, $\mathbf{I}_2$, and $\mathbf{J}$ precess independently about $\mathbf{H}$. For this case, the most appropriate choice of representation is the one which utilizes the basis vectors $|m_1,m_2,m_J\rangle$ since m_1, m_2, and m_J are "almost good" quantum numbers in this case. The required six quantum numbers will then be I_1, I_2, J, m_1, m_2, m_J.

(b) One nucleus primarily coupled to the rotational angular momentum, while the other is primarily coupled to the external field.

Suppose nucleus 1 is the one which is experiencing a strong field, and nucleus 2 is the one which is coupled to $\mathbf{J}$. Then $\mathbf{I}_1$ and $\mathbf{K}$ $(=\mathbf{I}_2+\mathbf{J})$ will precess independently about $\mathbf{H}$. In this case, therefore, the "almost good" quantum numbers will be m_1, m_K, and K. These and the "good" quantum numbers I_1, I_2, J, will form the six required quantum numbers.

(c) Both nuclei in a weak field, but one with a stronger quadrupole interaction than the other.

In this case the field is so weak that it is unable to decouple either of the nuclear angular momenta from the rotational angular momentum. If the coupling of $\mathbf{I}_2$ to $\mathbf{J}$ is much stronger than the coupling of $\mathbf{I}_1$ to $\mathbf{J}$, then $\mathbf{I}_2$ and $\mathbf{J}$ will precess about their resultant, $\mathbf{K}=\mathbf{I}_2+\mathbf{J}$, and $\mathbf{K}$ and $\mathbf{I}_1$ will precess their results, $\mathbf{F}=\mathbf{K}+\mathbf{I}_1$, and and finally $\mathbf{F}$ will precess about $\mathbf{H}$ with the magnetic quantum number m. Hence, the three "almost good" quantum numbers are K, F, and m.

(d) Any situation other than the previous three.

In this case no simple representation is good, but any one of them can be used, provided the secular equation is solved.

3. The Energy Levels

After choosing a representation, the matrix elements of the Hamiltonian in that representation can be calculated. The total magnetic quantum number m, i.e., the

[7] N. F. Ramsey, *Molecular Beams* (Oxford University Press, Oxford, England, 1956).

projection of the total angular momentum along the field axis, is a perfectly "good" quantum number in any representation. This simplifies the calculation of the matrix elements. The huge complete matrix is composed of submatrices of relatively small dimensions, each of them corresponding to a given value of m. In solving the secular equation for case (d), one must diagonalize each of these submatrices separately. In cases (a), (b), and (c), however, we only need to find the energy levels corresponding to a single m value and then treat m as a parameter to find all of the energy levels.

Most of the spectra in the present work can be analyzed by the coupling scheme (b). The molecules in this catagory are: LiCl, LiBr, LiI, NaI, KF, RbF, RbCl, CsCl. LiF and CsF can be treated by coupling scheme (a). The schemes (c) and (d) were not used in the analyses.

4. Energy Levels of KF

We begin by analyzing the spectrum of $K^{39}F^{19}$. This is the simplest molecule that can be treated by the coupling scheme (b). Fluorine has spin $\frac{1}{2}$ and, therefore, has no quadrupole moment. It is in a strong field. Potassium in $K^{39}F^{19}$ has a quadrupole interaction of -7.932 Mc/sec and the nuclear g factor is small (0.26097), so the fields used in the experiment are "weak." (The nuclear interaction with the field is of the order of 0.2 Mc/sec.)

The energy submatrix for a given m has a dimension of

$$(2I_F+1)(2I_K+1)=2\times 4=8.$$

In all cases where the nucleus which is strongly coupled to J has half-integral spin, degenerate perturbation theory should be used to determine the energy levels, because the zeroth-order energy values $E^0_{K=J+1/2,m_1}$ and $E^0_{K=J-1/2,m_1}$ are equal while the matrix element connecting them,

$$\langle K=J+\tfrac{1}{2}, m_1|H|K=J-\tfrac{1}{2}, m_1\rangle$$

does not vanish. Linear combinations of the two eigenstates $|K=J+\frac{1}{2}, m_1\rangle$ and $|K=J-\frac{1}{2}, m_1\rangle$ must be chosen:

$$\begin{aligned}|+\rangle&=a|K=J+\tfrac{1}{2}, m_1\rangle+b|K=J-\tfrac{1}{2}, m_1\rangle,\\ |-\rangle&=-b|K=J+\tfrac{1}{2}, m_1\rangle+b|K=J-\tfrac{1}{2}, m_1\rangle,\end{aligned}\tag{5}$$

and a and b should be determined by the condition: $\langle+|\mathcal{H}|-\rangle=0$, and the normalization condition.

The two new states are already orthogonal to each other and to $|K=J+\frac{3}{2}, m_1\rangle$ and $|K=J-\frac{3}{2}, m_1\rangle$. From these conditions a and b are found to be

$$a=\frac{1}{\sqrt{2}}(1+K)^{1/2},$$

$$b=\frac{1}{\sqrt{2}}(1-K)^{1/2},$$

where

$$K=z/(4-3z^2)$$

and

$$z=m/J.$$

Using this new set of basis vectors, the energy levels to second order with respect to the quadrupole interaction and external field interactions and to first order with respect to the spin-rotational interaction are

$$\begin{aligned}
E(J-\tfrac{3}{2}, \mp\tfrac{1}{2})\equiv E_{1,2}&=\pm\tfrac{1}{2}g_F\mu_N H-\frac{(eqQ)_K}{8}-mg_J\mu_N H+\tfrac{3}{2}g_K(1-\epsilon)z-\frac{3g_K^2\mu_N H(1-\epsilon)^2(1-z^2)}{(eqQ)_K}\pm\frac{c_F hm}{2}\\
E(J+\tfrac{3}{2}, \mp\tfrac{1}{2})\equiv E_{3,4}&=\pm\tfrac{1}{2}g_F\mu_N H-\frac{(eqQ)_K}{8}-mg_J\mu_N H-\tfrac{3}{2}g_K(1-\epsilon)z-\frac{3g_K^2\mu_N H(1-\epsilon)^2(1-z^2)}{(eqQ)_K}\pm\frac{c_F hm}{2}\\
E(-, \mp\tfrac{1}{2})\equiv E_{5,6}&=\pm\tfrac{1}{2}g_F\mu_N H+\frac{(eqQ)_K}{8}-mg_J\mu_N H+g_K(1-\epsilon)(1-\tfrac{3}{4}z^2)^{1/2}+\frac{3g_K^2\mu_N H^2(1-\epsilon)^2(1-z^2)}{(eqQ)_K}\pm\frac{c_F hm}{2}\\
E(-, \mp\tfrac{1}{2})\equiv E_{7,8}&=\pm\tfrac{1}{2}g_F\mu_N H+\frac{(eqQ)_K}{8}-mg_J\mu_N H-g_K(1-\epsilon)(1-\tfrac{3}{4}z^2)^{1/2}+\frac{3g_K^2\mu_N H^2(1-\epsilon)^2(1-z^2)}{(eqQ)_K}\pm\frac{c_F hm}{2},
\end{aligned}\tag{6}$$

where

$$\epsilon=g_J/g_{I_2}.$$

Hereafter, the first four energy levels in Eq. (6) will be called the "nondegenerate" levels, and the last four levels will be referred to as the "degenerate" levels.

5. Transition Frequencies of KF

In all of our low-frequency experiments the transitions follow the selection rules

$$\Delta m=\pm 1,\quad \Delta K=0,\quad \Delta m_1=0.\tag{7}$$

Using these selection rules, the frequencies of transition

corresponding to the energy levels Eq. (6) are

$$\begin{aligned}
\nu_{1,2}&=-\frac{g_J\mu_N H}{h}+\frac{3g_K\mu_N H(1-\epsilon)}{2Jh}\\
&\quad+\frac{6g_K{}^2\mu_N{}^2H^2(1-\epsilon)^2z}{J(eqQ)_K h}\pm\frac{c_F}{2},\\
\nu_{3,4}&=-\frac{g_J\mu_N H}{h}-\frac{3g_K\mu_N H(1-\epsilon)}{h}\\
&\quad+\frac{6g_K{}^2\mu_N{}^2H^2(1-\epsilon)^2z}{J(eqQ)_K h}\pm\frac{c_F}{2},\\
\nu_{5,6}&=-\frac{g_J\mu_N H}{h}-\frac{3g_K\mu_N H(1-\epsilon)z}{4Jh(1-\frac{3}{4}z^2)^{1/2}}\\
&\quad-\frac{6g_K{}^2\mu_N{}^2H^2(1-\epsilon)^2z}{J(eqQ)_K h}\pm\frac{c_F}{2},\\
\nu_{7,8}&=-\frac{g_J\mu_N H}{h}+\frac{3g_K\mu_N H(1-\epsilon)z}{4Jh(1-\frac{3}{4}z^2)^{1/2}}\\
&\quad-\frac{6g_K{}^2\mu_N{}^2H^2(1-\epsilon)^2z}{J(eqQ)_K h}\pm\frac{c_F}{2}.
\end{aligned}\tag{8}$$

Looking at the first-order terms in Eq. (8) we notice that the "degenerate" levels have a large z dependence, so large that multiple quantum transitions are not possible for these levels in our apparatus. The frequencies corresponding to these transitions will not be observable in our machine. There remain the "nondegenerate" levels 1–4 which do not have any z dependence in the first order of approximation. The large J dependence of these levels gives rise to the structure of the resonance curves. The second and higher order terms in these levels, which are z-dependent, only slightly change the width of the curves. As long as the width caused by different m's for a given J is within the coil width, these terms will not be important. For all of our molecules the second-order terms in Eq. (8) are completely negligible.

Neglecting the spin-rotational term for a moment, we notice two distinct frequencies in Eq. (8),

$$\nu_{I,II}=\frac{-g_J\mu_N H}{h}\pm\frac{3g_K\mu_N H(1-\epsilon)}{2Jh}.\tag{9}$$

The first term on the right-hand side of Eq. (9) is the rotational term, and the second is the nuclear term. For the most probable value of J, these two terms are approximately of the same order of magnitude. Depending on the sign of g_J, one of the two frequencies in Eq. (9) is much larger than the other one. Since the deflection of the beam at the detector after transition is linearly proportional to the effective g factor, only one of the two frequencies in Eq. (9) will be observable. The quantitative description of the deflectability factor in the next section will justify the above qualitative argument.

The effect of the spin-rotational terms $\pm\frac{1}{2}c_H$ in Eq. (8) is simply to widen the resonance and possibly (for large enough values of c_H) split the resonance into two branches, as was observed in the CsF spectrum. Therefore, for simplifying the analysis, we omit the c_H factor now, remembering that for the correct determination of the theoretical natural widths of the resonances, the c_H constant must be added to the width obtained from the J-dependent nuclear term.

6. The Deflectability Weighting Factor

The intensity function of ν, $I(\nu)$, is a product of three functions:

1. the Boltzmann distribution function of J given by Eq. (3),
2. the density of the transitions $|dJ/d\nu|$

$$|dJ/d\nu|=\text{constant}\ J^2,\tag{10}$$

3. the deflectability weighting factor $D(J)$ which will presently be defined and developed.

Cederberg and Ramsey[2] have shown that in the classical limit of high J, the fraction of the molecules which undergo a change in m (per unit of angular momentum) between $\Delta m/J$ and $\Delta m/J+d(\Delta m/J)$ is $P(\Delta m/J)d(\Delta m/J)$, where $P(\Delta m/J)$ is given by

$$\begin{aligned}
P\left(\frac{\Delta m}{J}\right)&=\frac{1}{|4\sin\tfrac{1}{2}\theta|}\quad\text{for}\quad\left|\frac{\Delta m}{J}\right|<2|\sin\tfrac{1}{2}\theta|\\
&=0\qquad\text{for}\quad\left|\frac{\Delta m}{K}\right|\geq 2|\sin\tfrac{1}{2}\theta|,
\end{aligned}\tag{11}$$

$$\sin\tfrac{1}{2}\theta=\frac{(g\mu_N H/2h)\sin\{(\pi Lc/v)[[\nu-(g\mu_N H/h)]^2+(g\mu_N H'/2h)^2]^{1/2}\}}{[[\nu-(g\mu_N H/h)]^2+(g\mu_N H'/2h)]^{1/2}}.\tag{12}$$

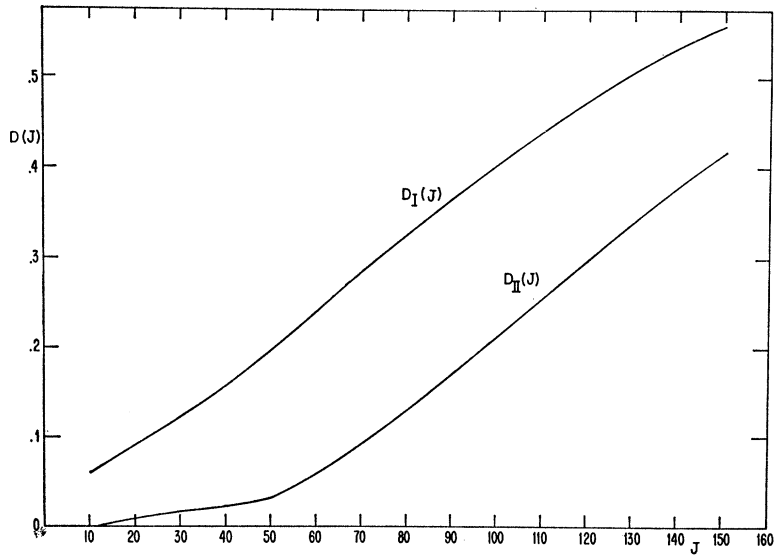

FIG. 1. The deflectability weighting factor for potassium fluoride.

H' is the magnitude of the radiofrequency magnetic field, and v is the velocity of the molecule in the beam. For an "infinitely" long coil, at resonance Eq. (12) reduces to

$$\sin\tfrac{1}{2}\theta=\sin((\pi Lc/v)(g\mu_N H/2h)). \tag{13}$$

The deflection S of the beam at the detector position, after transition, is[7]

$$S=(\Delta\mu/m_M v^2)(\partial H/\partial z)l_B(l_4+\tfrac{1}{2}l_B), \tag{14}$$

where $\Delta\mu$ is the change in the component of the magnetic moment along the external field, $\partial H_B/\partial Z$ is the gradient of the B field $\cong$26 000 G cm^{-1}, l_B is the length of the B magnet $\cong$38.2 cm, and l_4 is the distance from the B magnet to the detector $\cong$66 cm. The change $\Delta\mu$ is given by

$$\Delta\mu=Jg\mu_N|\Delta m/J|. \tag{15}$$

Making this substitution, Eq. (14) reads

$$S=S_1 Jg|\Delta m/J|, \tag{16}$$

where S_1 is

$$S_1=(\mu_N/m_M v^2)(\partial H_B/\partial Z)l_B(l_4+\tfrac{1}{2}l_B). \tag{17}$$

If we use the most probable velocity in the beam, $1.22\alpha=1.22(2kT/m_M)^{1/2}$, for v and also substitute the rest of the constants in Eq. (17), S_1 will turn out to be

$$S_1=\frac{410}{T}\text{ mils}\quad(1\text{ mil}=0.001\text{ in.}).$$

Therefore,

$$S=(410/T)Jg|\Delta m/J|. \tag{18}$$

The beam shape at the detector is trapezoidal.[7] For the sake of mathematical simplicity we approximate the beam shape function by a Gaussian function of width 1 mil (the normal beam width). The undeflected shape function is, therefore

$$I(x)=(2\pi)^{-1/2}e^{-\frac{1}{2}x^2}, \tag{19}$$

where x is the horizontal distance in mils from the center of the detector. The displaced shape function (assuming that the shape is not distorted after deflection) is

$$I(x,S)=(2\pi)^{-1/2}e^{-\frac{1}{2}(x-S)^2}. \tag{20}$$

From these equations and for a detector of width $w_d=1$ mil, the total intensity detected before deflection is

$$I_{\text{undeflected}}=\frac{1}{(2\pi)^{1/2}}\int_{-\frac{1}{2}}^{+\frac{1}{2}}e^{-\frac{1}{2}x^2}dx, \tag{21}$$

and the intensity after deflection is

$$I_{\text{deflected}}=\frac{1}{(2\pi)^{1/2}}\int_{-\frac{1}{2}}^{+\frac{1}{2}}e^{-\frac{1}{2}(x-S)^2}dx. \tag{22}$$

The fraction of molecules deflected will, therefore, be

$$D(S)=1-\int_{-\frac{1}{2}}^{+\frac{1}{2}}e^{-\frac{1}{2}(x-S)^2}dx\Big/\int_{-\frac{1}{2}}^{+\frac{1}{2}}e^{-\frac{1}{2}x^2}dx. \tag{23}$$

This function is approximately

$$D(S)\cong 1-(1+0.04S^2+\cdots)e^{-\frac{1}{2}S^2}. \tag{24}$$

Multiplying this function by the Cederberg and Ramsey function, Eq. (13), and integrating over $\Delta m/J$ will give the deflectability weighting factor as a function of J:

$$D(J)=\int_0^{2\sin\frac{1}{2}\theta}\frac{1}{2\sin\frac{1}{2}\theta}D(S)d\left(\frac{\Delta m}{J}\right), \tag{25}$$

where S is given by Eq. (18) as a function of J and

$\Delta m/J$. Carrying out the integration, $D(J)$ will become

$$D(J)\cong 1-0.00153(T/g_J \sin\tfrac{1}{2}\theta)\ \mathrm{erf}(580 g_J \sin\tfrac{1}{2}\theta/T). \quad (26)$$

To a very good approximation, for all of our molecules this function is linear in J. This linear approximation will be used in the determination of the width of the resonances. For determination of the peak of the resonances, which are of primary interest to us, Eq. (26) itself will be used to give slightly more accurate results.

Figure 1 is a plot of the function $D(J)$ versus J for the molecule KF. The two branches of Fig. 1 correspond to the two frequencies given by Eq. (9). It can be seen from these curves that the deflectability factor is approximately linear in J.

7. The Intensity Function

The total intensity function, a product of the Boltzmann distribution function, Eq. (3), the transition density function, Eq. (10), and the deflectability weighting function, Eq. (26), can now be plotted against J and $J_{\max}$ be determined. In doing this, we first use the value of g_J as given by the ionic model (see Sec. III). The value of $J_{\max}$ determined in this way and the $\nu_{\max}$, corresponding to the peak of the experimental resonance curve can then be used in Eq. (9) and g_J be calculated.

This determined value of g_J can then be used in Eq. (26) and the above procedure repeated to give a better value of g_J. Repeating this trial and error procedure a few times determines the value of g_J. Once g_J is known, Eq. (9) may be solved for J as a function of ν, and the intensity versus ν may be plotted. Figure 2 shows this plot for KF and Fig. 3 shows the plot of the observed experimental KF resonance. The spin-rotational interaction has been omitted in this theoretical plot. This omission merely causes the two curves to look narrower, but would not shift the centers of them. This figure shows that the ratio of strength of the two branches is about three to one. This ratio is even higher for the other molecules since the rf current used was close to optimum for the big branch and, therefore, off optimum for the small branch.

This result shows that we are justified in assuming that the observed resonance is $I(\nu_{\mathrm{I}})$. The other branch, $I(\nu_{\mathrm{II}})$, dies out in the noise.

The foregoing analysis can be used for other molecules obeying the coupling scheme (b), once their energy levels have been determined.

8. Analysis of $Rb^{85}F^{19}$ Spectrum

Rubidium 85 has spin $\frac{5}{2}$. This gives rise to $(2\times\frac{5}{2}+1)\times(2\times\frac{1}{2}+1)=12$ distinct energy levels for a given m. Using the same procedure as for KF with slight modifications, the energy levels of this molecule (to the same order of approximation as for KF) are:

$$E(J-\tfrac{5}{2},\mp\tfrac{1}{2})\equiv E_{1,2}=\pm\tfrac{1}{2}g_{\mathrm{F}}\mu_N H-\frac{(eqQ)_{\mathrm{Rb}}}{8}-mg_J\mu H+\frac{5m}{2J}\mu_N g_{\mathrm{Rb}}H(1-\epsilon)-\frac{25}{3}\frac{g_{\mathrm{Rb}}^2\mu_N^2H^2(1-\epsilon)^2(1-z^2)}{(eqQ)_{\mathrm{Rb}}}\pm\frac{mc_{\mathrm{F}}h}{2},$$

$$E(J-\tfrac{3}{2},\mp\tfrac{1}{2})\equiv E_{3,4}=\pm\tfrac{1}{2}g_{\mathrm{F}}\mu_N H+\frac{(eqQ)_{\mathrm{Rb}}}{40}-mg_J\mu H+\frac{3m}{2J}\mu_N g_{\mathrm{Rb}}H(1-\epsilon)-\frac{55}{3}\frac{g_{\mathrm{Rb}}^2\mu_N^2H^2(1-\epsilon)^2(1-z^2)}{(eqQ)_{\mathrm{Rb}}}\pm\frac{mc_{\mathrm{F}}h}{2},$$

$$E(+,\mp\tfrac{1}{2})\equiv E_{5,6}=\pm\tfrac{1}{2}g_{\mathrm{F}}\mu_N H+\frac{(eqQ)_{\mathrm{Rb}}}{10}-mg_J\mu H$$
$$+\tfrac{3}{2}\mu_N g_{\mathrm{Rb}}H(1-\epsilon)\left(1-\frac{8}{9}z^2\right)^{1/2}+\frac{80}{3}\frac{g_{\mathrm{Rb}}^2\mu_N^2H^2(1-\epsilon)^2(1-z^2)}{(eqQ)_{\mathrm{Rb}}}\pm\frac{mc_{\mathrm{F}}h}{2},$$

$$E(-,\mp\tfrac{1}{2})\equiv E_{7,8}=\pm\tfrac{1}{2}g_{\mathrm{F}}\mu_N H+\frac{(eqQ)_{\mathrm{Rb}}}{10}-mg_J\mu H$$
$$-\tfrac{3}{2}\mu_N g_{\mathrm{Rb}}H(1-\epsilon)\left(1-\frac{8}{9}z^2\right)^{1/2}+\frac{80}{3}\frac{g_{\mathrm{Rb}}^2\mu_N^2H^2(1-\epsilon)^2(1-z^2)}{(eqQ)_{\mathrm{Rb}}}\pm\frac{mc_{\mathrm{F}}h}{2},$$

$$E(J+\tfrac{3}{2},\mp\tfrac{1}{2})\equiv E_{9,10}=\pm\tfrac{1}{2}g_{\mathrm{F}}\mu_N H+\frac{(eqQ)_{\mathrm{Rb}}}{40}-mg_J\mu H-\frac{3m}{2J}\mu_N g_{\mathrm{Rb}}H(1-\epsilon)-\frac{55}{3}\frac{g_{\mathrm{Rb}}^2\mu_N^2H^2(1-\epsilon)^2(1-z^2)}{(eqQ)_{\mathrm{Rb}}}\pm\frac{mc_{\mathrm{F}}h}{2},$$

$$E(J+\tfrac{5}{2},\mp\tfrac{1}{2})\equiv E_{11,12}=\tfrac{1}{2}g_{\mathrm{F}}\mu_N H-\frac{(eqQ)_{\mathrm{Rb}}}{8}-mg_J\mu_N H-\frac{5m}{2J}\mu_N g_{\mathrm{Rb}}H(1-\epsilon)-\frac{25}{3}\frac{g_{\mathrm{Rb}}^2\mu_N^2H^2(1-\epsilon)^2(1-z)^2}{(eqQ)_{\mathrm{Rb}}}\pm\frac{mc_{\mathrm{F}}h}{2}. \quad (27)$$

The frequencies corresponding to these energy levels are:

$$\begin{aligned}
\nu_{1,2}&=-\frac{g_J\mu_N H}{h}+\frac{5}{2J}\frac{g_{\mathrm{Rb}}\mu_N H(1-\epsilon)}{h}\pm\frac{c_{\mathrm{F}}}{2}+\frac{50}{3}\frac{g_{\mathrm{Rb}}{}^2\mu_N{}^2(1-\epsilon)^2H^2z}{3(eqQ)_{\mathrm{Rb}}Jh},\\
\nu_{3,4}&=-\frac{g_J\mu_N H}{h}+\frac{3}{2J}\frac{g_{\mathrm{Rb}}\mu_N H(1-\epsilon)}{h}\pm\frac{c_{\mathrm{F}}}{2}+\frac{110}{3}\frac{g_{\mathrm{Rb}}{}^2\mu_N{}^2H^2(1-\epsilon)^2z}{(eqQ)Jh},\\
\nu_{5,6}&=-\frac{g_J\mu_N H}{h}+\frac{4}{3J}\frac{g_{\mathrm{Rb}}(1-\epsilon)z\mu_N H}{h(1-(8/9)z^2)^{1/2}}\pm\frac{c_{\mathrm{F}}}{2}+\frac{160}{3J}\frac{g_{\mathrm{Rb}}{}^2\mu_N{}^2(1-\epsilon)^2H^2}{(eqQ)_{\mathrm{Rb}}h},\\
\nu_{7,8}&=-\frac{g_J\mu_N H}{h}+\frac{4}{3J}\frac{g_{\mathrm{Rb}}(1-\epsilon)z\mu_N H}{h(1-(8/9)z^2)^{1/2}}\pm\frac{c_{\mathrm{F}}}{2}+\frac{160}{3J}\frac{g_{\mathrm{Rb}}{}^2\mu_N{}^2(1-\epsilon)^2H^2}{(eqQ)_{\mathrm{Rb}}h},\\
\nu_{9,10}&=-\frac{g_J\mu_N H}{h}-\frac{3}{2J}\frac{g_{\mathrm{Rb}}(1-\epsilon)H\mu_N}{h}\pm\frac{c_{\mathrm{F}}}{2}+\frac{110}{3}\frac{g_{\mathrm{Rb}}{}^2(1-\epsilon)^2z\mu_N{}^2H^2}{(eqQ)_{\mathrm{Rb}}Jh},\\
\nu_{11,12}&=-\frac{g_J\mu_N H}{h}-\frac{5}{2J}\frac{g_{\mathrm{Rb}}\mu_N H(1-\epsilon)}{h}\pm\frac{c_{\mathrm{F}}}{2}+\frac{50}{3}\frac{g_{\mathrm{Rb}}{}^2(1-\epsilon)^2z\mu_N{}^2H^2}{(eqQ)_{\mathrm{Rb}}Jh}.
\end{aligned}\tag{28}$$

With reference to the arguments given for KF, the following observations can be made.

1. Frequencies ν_9–ν_{12} are not important due to small effective g's.
2. Frequencies ν_5–ν_8 are not important because of the large z dependence which rules out the possibility of multiple transitions.
3. Frequencies ν_1–ν_4 *are* important, and the peak of the resonance corresponds to the average of these terms, i.e.,

$$\bar{\nu}_{\mathrm{RbF}}=-\frac{g_J\mu_N H}{h}+\frac{2g_{\mathrm{Rb}}\mu_N H(1-\epsilon)}{Jh}\pm\frac{c_{\mathrm{F}}}{2},\tag{29}$$

again omitting the small second-order quadrupole terms.

The peak of the experimental resonance curve corresponds to $\bar{\nu}$. Using Eq. (29) together with the analysis of the previous section, we get the g_J value of $\mathrm{Rb}^{85}\mathrm{F}^{19}$.

9. Analysis of $\mathrm{Li}^7\mathrm{Cl}$, $\mathrm{Li}^6\mathrm{Cl}$, LiBr, LiI, NaI, RbCl, and CsCl Spectra

Consider, first, the $\mathrm{Li}^7\mathrm{Cl}$ molecule. Both nuclei in this molecule possess quadrupole moments. However, the quadrupole interaction of the lithium nucleus (nucleus 1) is so small that it is effectively in a strong external field, whereas the chlorine nucleus (nucleus 2) is in a weak field because of its large quadrupole interaction. This molecule can, therefore, be treated by the coupling case (b), too. Using the Hamiltonian of Eq. (2), the energy levels can be calculated. In this calculation the matrix element

$$\langle m_1,K,m_K|\,3(\mathbf{I}_1\cdot\mathbf{J})^2+\tfrac{3}{2}(\mathbf{I}_1\cdot\mathbf{J})-I_1{}^2J^2\,|m_1',K,m_K'\rangle$$

must be found. This has been done by Pinkerton[1]:

$$\langle m_1,K,m_K|\,3(\mathbf{I}_1\cdot\mathbf{J})^2+\tfrac{3}{2}(\mathbf{I}_1\cdot\mathbf{J})-I_1{}^2J^2\,|m_1',K,m_K'\rangle=C(K,J,I_2)\langle m_1,K,m_K|\,3(\mathbf{I}_1\cdot\mathbf{K})^2+\tfrac{3}{2}(\mathbf{I}_1\cdot\mathbf{K})-I_1{}^2K^2\,|m_1',K,m_K'\rangle,$$

where

$$\begin{aligned}
C(K,J,I_2)=\frac{1}{K(2K-1)}\Bigg\{3\left[\frac{K(K+1)+J(J+1)-I_2(I_2+1)}{2(K+1)}\right]^2\\
+3\frac{(K+1-I_2+J)(K+1+I_2-J)(I_2+J+2+K)(I_2+J-K)}{4(K+1)^2(2K+3)}-J(J+1)\Bigg\}.
\end{aligned}$$

For large J, $C(K,J,I_2)\cong 1$. The determination of the above matrix element was not required for the previous cases (KF and RbF), since in those cases one nucleus had no quadrupole moment.

TABLE I. The coefficients of Eqs. (30) and (31).

	K	m_1		a_1	a_2	a_3	a_4	a_5	b_1	b_2	b_3
J	$-\frac{3}{2}$	$-\frac{3}{2}$		$+\frac{3}{2}$	$+1$	-1	$+1$	$+1$	$+1$	-1	$(9/128)z-(21/128)z^3$
J	$+\frac{3}{2}$	$-\frac{3}{2}$		$+\frac{3}{2}$	-1	-1	$+1$	$+1$	-1	-1	$(9/128)z-(21/128)z^3$
J	$-\frac{3}{2}$	$-\frac{1}{2}$		$+\frac{1}{2}$	$+1$	$+1$	-1	$+1$	$+1$	$+1$	$(27/128)z^3-(15/128)z$
J	$+\frac{3}{2}$	$-\frac{1}{2}$		$+\frac{1}{2}$	-1	$+1$	-1	$+1$	-1	$+1$	$(27/128)z^3-(15/128)z$
J	$-\frac{3}{2}$	$+\frac{1}{2}$		$-\frac{1}{2}$	$+1$	$+1$	$+1$	-1	$+1$	$+1$	$(15/128)z-(27/128)z^3$
J	$+\frac{3}{2}$	$+\frac{1}{2}$		$-\frac{1}{2}$	-1	$+1$	$+1$	-1	-1	$+1$	$(15/128)z-(27/128)z^3$
J	$-\frac{3}{2}$	$+\frac{3}{2}$		$-\frac{3}{2}$	$+1$	-1	-1	-1	$+1$	-1	$(21/128)z^3-(9/128)z$
J	$+\frac{3}{2}$	$+\frac{3}{2}$		$-\frac{3}{2}$	-1	-1	-1	-1	-1	-1	$(21/128)z^3-(9/128)z$

The "nondegenerate" energy levels are

$$E(K,m_1)=a_1g_{\mathrm{Li}}\mu_NH-\frac{(eqQ)_{\mathrm{Cl}}}{8}-mg_J\mu_NH+a_2\tfrac{3}{2}g_{\mathrm{Cl}}\mu_NH(1-\epsilon)z+a_3\frac{(eqQ)_{\mathrm{Li}}}{16}(3z^2-1)$$
$$-\frac{4g_{\mathrm{Cl}}{}^2\mu_N{}^2H^2(1-\epsilon)^2(1-z^2)}{(eqQ)_{\mathrm{Cl}}}+a_4\frac{3}{64}\frac{(eqQ)_{\mathrm{Li}}{}^2z^2(1-z)^2}{g_{\mathrm{Li}}\mu_NH}+a_5\frac{3}{512}\frac{(eqQ)_{\mathrm{Li}}{}^2(1-z^2)}{g_{\mathrm{Li}}\mu_NH}, \quad (30)$$

where $a_1, \cdots, a_5$ are given by Table I. The corresponding frequencies are

$$\nu(K,m_1)=-\frac{g_J\mu_NH}{h}+b_1\frac{3}{2J}\frac{g_{\mathrm{Cl}}(1-\epsilon)\mu_NH}{h}+b_2\frac{3}{8}\frac{(eqQ)_{\mathrm{Li}}z}{Jh}+\frac{8g_{\mathrm{Cl}}{}^2\mu_N{}^2H^2(1-\epsilon)^2z}{J(eqQ)_{\mathrm{Cl}}h}+b_3\frac{(eqQ)_{\mathrm{Li}}{}^2}{g_{\mathrm{Li}}\mu_NHJh}, \quad (31)$$

where b_1, b_2, b_3 are given by Table I.

The "degenerate" levels which are not given here will not undergo transition. The second-order terms in Eq. (31) are negligible. The first-order Li_7-quadrupole term, although not negligible, will not cause a shift in the center of the resonance. The first-order Cl_{35}-nuclear term, however, will cause such a shift, and its effect is completely similar to that in KF. Therefore, the analysis of the previous section is entirely applicable to this molecule and to Li^6Cl, LiBr, and CsCl. Equation (9) can be used for all these molecules. With regard to LiI, NaI, and RbCl where the "nucleus in the weak field" has spin $\frac{5}{2}$, Eq. (29) must be used instead of Eq. (9) to give the average effective frequency.

10. Analysis of LiF and CsF Spectra

For these molecules, where both nuclei are effectively in strong fields, coupling scheme (a) gives the following energy levels:

$$E(m_{\mathrm{F}}=\mp\tfrac{1}{2},\ m_{\mathrm{Li}}=-\tfrac{3}{2})\equiv E_{1,2}=\pm\tfrac{1}{2}g_{\mathrm{F}}\mu_NH+\tfrac{3}{2}g_{\mathrm{Li}}\mu_NH-m_Jg_J\mu_NH\pm(\tfrac{1}{2}c_{\mathrm{F}})hm_J$$
$$-\tfrac{1}{16}(eqQ)_{\mathrm{Li}}(3z^2-1)+\frac{3}{512}\frac{(eqQ)_{\mathrm{Li}}{}^2}{g_{\mathrm{Li}}\mu_NH}(1+6z^2-7z^4),$$

$$E(\mp\tfrac{1}{2},\ -\tfrac{1}{2})\equiv E_{3,4}=\pm\tfrac{1}{2}g_{\mathrm{F}}\mu_NH+\tfrac{1}{2}g_{\mathrm{Li}}\mu_NH-m_Jg_J\mu_NH\pm(\tfrac{1}{2}c_{\mathrm{F}})hm_J$$
$$+\tfrac{1}{16}(eqQ)_{\mathrm{Li}}(3z^2-1)+\frac{3}{512}\frac{(eqQ)_{\mathrm{Li}}{}^2}{g_{\mathrm{Li}}\mu_NH}(1-10z^2+9z^4),$$

$$E(\mp\tfrac{1}{2},\ +\tfrac{1}{2})\equiv E_{5,6}=\pm\tfrac{1}{2}g_{\mathrm{F}}\mu_NH-\tfrac{1}{2}g_{\mathrm{Li}}\mu_NH-m_Jg_J\mu_NH\pm(\tfrac{1}{2}c_{\mathrm{F}})hm_J \quad (32)$$
$$+\tfrac{1}{16}(eqQ)_{\mathrm{Li}}(3z^2-1)-\frac{3}{512}\frac{(eqQ)_{\mathrm{Li}}{}^2}{g_{\mathrm{Li}}\mu_NH}(1-10z^2+9z^4),$$

$$E(\mp\tfrac{1}{2},\ +\tfrac{3}{2})\equiv E_{7,8}=\pm\tfrac{1}{2}g_{\mathrm{F}}\mu_NH-\tfrac{3}{2}g_{\mathrm{Li}}\mu_NH-m_Jg_J\mu_NH\pm(\tfrac{1}{2}c_{\mathrm{F}})hm_J$$
$$-\tfrac{1}{16}(eqQ)_{\mathrm{Li}}(3z^2-1)-\frac{3}{512}\frac{(eqQ)_{\mathrm{Li}}{}^2}{g_{\mathrm{Li}}\mu_NH}(1+6z^2-7z^4),$$

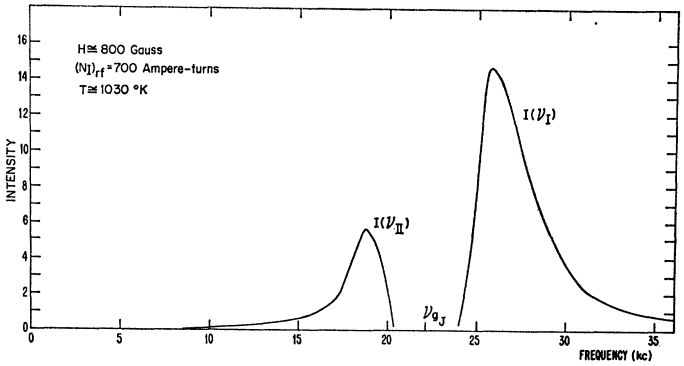

FIG. 2. Theoretical shape of KF rotational resonance (excluding spin-rotational interaction). $H\cong 800$ G, $(NI)_{rf}\cong 700$ ampere-turns, $T\cong 1030°$K.

and the corresponding frequencies are:

$$\begin{aligned}
\nu_{1,2}&=-\frac{g_J\mu_N H}{h}-\frac{3}{8}\frac{z}{J}\frac{(eqQ)_{\mathrm{Li}}}{h}\pm\frac{c_{\mathrm{F}}}{2}+\frac{3}{128}\frac{(eqQ)_{\mathrm{Li}}^2(3z-7z^3)}{g_{\mathrm{Li}}\mu_N HJh},\\
\nu_{3,4}&=-\frac{g_J\mu_N H}{h}+\frac{3}{8}\frac{z}{J}\frac{(eqQ)_{\mathrm{Li}}}{h}\pm\frac{c_{\mathrm{F}}}{2}-\frac{3}{128}\frac{(eqQ)_{\mathrm{Li}}^2(5z-9z^3)}{g_{\mathrm{Li}}\mu_N HJh},\\
\nu_{5,6}&=-\frac{g_J\mu_N H}{h}+\frac{3}{8}\frac{z}{J}\frac{(eqQ)_{\mathrm{Li}}}{h}\pm\frac{c_{\mathrm{F}}}{2}+\frac{3}{128}\frac{(eqQ)_{\mathrm{Li}}^2(3z^2-7z^3)}{g_{\mathrm{Li}}\mu_N HJh},\\
\nu_{7,8}&=-\frac{g_J\mu_N H}{h}-\frac{3}{8}\frac{z}{J}\frac{(eqQ)_{\mathrm{Li}}}{h}\pm\frac{c_{\mathrm{F}}}{2}-\frac{3}{128}\frac{(eqQ)_{\mathrm{Li}}^2(3z^2-7z^3)}{g_{\mathrm{Li}}\mu_N HJh}.
\end{aligned}\tag{33}$$

Selection rules $\Delta m_J=\pm 1$ and $\Delta m_1=\Delta m_2=0$ have been used in finding these frequencies.

As can be seen from Eq. (33), the central frequency corresponds to the rotational g value. The other terms only affect the natural width of the resonance curves. For CsF, the ratio of the cesium first-order quadrupole term to the cesium nuclear term in Eq. (32) is about $\frac{1}{4}$. Therefore, coupling case (a) does not give the exact answer, since there might be some mixture of coupling scheme (b), and a larger error is associated with the CsF g value. Table II is a tabulation of the g_{peak} values which correspond to the peaks of the observed resonances as given by Eqs. (9) and (29) and the calculated g_J values. For LiF and CsF the two values are, of course, the same.

TABLE II. Effective and rotational g values.

Molecule	$g_{\mathrm{exp\ peak}}$	g_J (corrected)
Li^7F^{19}	0.07367 ±0.00050	0.07367±0.00050
Li^7Cl^{35}	0.10097 ±0.00017	0.0848 ±0.0032
Li^6Cl^{35}	0.1208 ±0.0011	0.1042 ±0.0033
Li^7Br^{79}	0.13768 ±0.00082	0.0911 ±0.0039
Li^7I^{127}	0.15121 ±0.00089	0.1068 ±0.0089
$Na^{23}I^{127}$	0.05015 ±0.00052	0.0268 ±0.0047
$K^{39}F^{19}$	0.04245 ±0.00023	0.0364 ±0.0012
$Rb^{85}F^{19}$	0.05789 ±0.00090	0.0441 ±0.0028
$Rb^{85}Cl^{35}$	0.027191±0.000072	0.0183 ±0.0018
$Cs^{133}F^{19}$	0.06207 ±0.00034	0.0621 ±0.0055
$Cs^{133}Cl^{35}$	0.026698±0.000071	0.0212 ±0.0011

11. The Natural Width of the Resonance Curves

The approximate form of the intensity function for coupling case (b) is

$$I(\nu)=\mathrm{constant}J^4(\nu)\exp(-\tfrac{1}{2}J^2(\nu)/J_m^2).\tag{34}$$

This is the product of the three previously discussed functions (Sec. II.7), except that instead of the deflectability weighting factor, Eq. (26), a linear function of J (i.e., constant$\times J$) has been substituted. (See the remark at the end of Sec. 6.)

In the intensity function Eq. (34)

$$I_{\max}\text{ occurs at }J=2J_m,$$
$$I_{\frac{1}{2}\max}\text{ cocurs at }J=1.236J_m.$$

Therefore, for spin $\frac{3}{2}$,

$$\begin{aligned}
\nu_{\max}&=\frac{g_J\mu_N H}{h}+\frac{1.5g_w\mu_N H(1-\epsilon)}{2J_m h},\\
\nu_{\frac{1}{2}\max}&=\frac{g_J\mu_N H}{h}+\frac{1.5g_w\mu_N H(1-\epsilon)}{1.236J_m h},
\end{aligned}\tag{35}$$

where g_w is the nuclear g factor of the nucleus in the weak field. The natural line breadth is given by twice the difference of the two equations in Eq. (35) plus the spin-rotational constant of the nucleus in the strong

field C_s.

$$(\Delta\nu)_{\text{natural}} \cong \frac{0.93 g_w \mu_N H(1-\epsilon)}{J_m h}. \quad (36)$$

For spin $\frac{5}{2}$ cases, Eqs. (28) and (34) give

$$\begin{aligned}
\nu_{\max_1} &= \frac{g_J \mu_N H}{h} + \frac{1.5 g_w \mu_N H(1-\epsilon)}{2 J_m h}, \\
\nu_{\frac{1}{2}\max_1} &= \frac{g_J \mu_N H}{h} + \frac{1.5 g_w \mu_N H(1-\epsilon)}{1.236 J_m h}, \\
\nu_{\max_2} &= \frac{g_J \mu_N H}{h} + \frac{2.5 g_w \mu_N H(1-\epsilon)}{2 J_m h}, \\
\nu_{\frac{1}{2}\max_2} &= \frac{g_J \mu_N H}{h} + \frac{2.5 g_w \mu_N H(1-\epsilon)}{1.236 J_m h}.
\end{aligned} \quad (37)$$

The total full width at half-height is

$$\begin{aligned}
\Delta\nu_{\text{natural}} = &(\nu_{\max_1} - \nu_{\frac{1}{2}\max_1}) + (\nu_{\max_2} - \nu_{\max_1}) \\
&+ (\nu_{\max_2} - \nu_{\frac{1}{2}\max_2}) + c_s. \quad (38)
\end{aligned}$$

Using Eq. (38), Eq. (37) reduces to

$$\Delta\nu_{\text{natural}} = \frac{1.74 g_w \mu_N H(1-\epsilon)}{J_m h} + c_s. \quad (39)$$

For coupling case (a), Eqs. (33) shows that the width is simply given by

$$\Delta\nu_{\text{natural}} = c_F. \quad (40)$$

The natural width should be combined with the width due to rf coil. Assuming a Gaussian shape function for the molecule and the coil, one can arrive at the following relationship

(theoretical width) = (natural width)
$+\frac{1}{2}$(coil width)$\times$(coil width)/(natural width).

Table III shows a good agreement between the theoretical and the observed widths in most cases. This is a confirmation of the validity of the assumptions used in deriving the total intensity function. If both branches of Fig. 1 were of the same strength, the resonance curves would have been much wider. The observed width can be explained only if we consider one of the two branches of Fig. 2 and not both.

For the spin-rotational constant of the fluorine nucleus in LiF, the electric and the magnetic resonance methods give two different values.[8] Note, in Table III, that the observed width in the present experiment agrees more with the width calculated from the magnetic resonance value of the spin-rotational constant than from the electric resonance value, although the latter is usually considered to be more reliable.

[8] W. A. Nierenberg and N. F. Ramsey, Phys. Rev. **72**, 1075 (1947); R Braunstein and J. W. Trischka, *ibid.*, **90**, 348 (1953).

TABLE III. Theoretical and experimental linewidths.

Molecule	Field (gauss)	$(\Delta\nu)_{\text{theory}}$	$(\Delta\nu)_{\text{exp}}$
LiF	1315	{23.6 (from magnetic resonance) 35.1 (from electric resonance)}	24.0
LiCl	883	16.5	14.4
LiCl	943	17.3	14.6
LiCl	1330	22.1	18.9
LiBr	682	27.2	50.6
LiI	682	37.4	52.5
NaI	1375	37.2	41.0
NaI	1800	49.7	46.5
KF	799	16.8	18.7
KF	883	17.4	19.4
KF	1270	17.6	18.7
KF	1830	22.6	25.0
KF	2070	24.0	24.0
RbF	681	24.2	21.0
RbF	1495	39.1	38.5
RbCl	1330	16.9	18.2
CsF	799	13.0	13.0
CsCl	1330	8.5	7.0

13. Discussion of Errors

The peak of the experimental curve was determined by taking the average of the peaks of several resonances. The error involved in this determination is the usual rms error and is mainly due to the shifts in the peaks of the curves caused by the noise. This error is of the order of 1%.

The next step is to determine $\nu_{\text{effective}}$ as defined by Eq. (9) from the experimental curves. If the theory given is absolutely correct, the peak of the experimental curve *is* $\nu_{\text{effective}}$. However, because of the restrictive assumptions made in arriving at the theory, a relatively large error is involved in identifying the peak of the experimental curve as $\nu_{\text{effective}}$. For instance, there are the following sources for this error.

There may be deviations from the Boltzmann function because of the possibility of some of the deflected molecules being cut off by magnetic pole tips or other parts of the apparatus. This effect which may be large for extremely large values of J will not be too large for the effective values of J since for these the deflections are so small that the probability of molecules hitting the pole faces and disappearing from the beam is small. Another effect is due to the lack of symmetry in the theoretical curve. Because of this asymmetry, the broadening factors such as the coil width and quadrupole interactions will tend to displace the top of the curve. This effect is estimated to be of the order of 5%.

There are also the following facts which were neglected in deriving the theory: The shape of the beam will be distorted upon deflection. The beam-shape function is not Gaussian. The Cederberg and Ramsey theory is not exactly applicable due to the second-order m-dependent effects. Considering all these effects and allowing for possible other unknown effects, the uncertainty in the correction value (i.e., $g_{\text{peak}} - g_J$) is estimated to be about 20%. Since the correction is large, the uncertainty adds

greatly to the final estimated error. The large magnitude of the correction also opens the possibility for an even larger error if the interpretation of the result is wrong. This possibility does not exist in the case of LiF and other molecules with small quadrupole interactions for which such large corrections are not required.

The partial but incomplete agreement between the theoretical and experimental widths of the resonances confirms in part the use of the theory but also indicates the limitations.

Once $g_{\text{effective}}$ is determined, g_J can be calculated from Eq. (9). There is a relatively small error of the order of one percent introduced in this calculation due to the uncertainty in J.

III. DISCUSSION OF RESULTS

1. The Rotational Magnetic Moment

The ionic model of the alkali-halide molecules gives a rotational g factor

$$g_{\text{ionic}}=1/M_+-1/M_-, \tag{41}$$

where M_+ and M_- are the masses of the alkali and the halogen ions expressed in atomic units.

To the ionic g value must be added the contribution due to the valence electrons. This contribution, the so-called high-frequency term, is given by[9]

$$g_e=\frac{2\mu_0}{\mu_N I}\sum_n{}'\frac{|\langle n|L_x\hbar|0\rangle|^2}{E_n-E_0}, \tag{42}$$

where μ_0 is the Bohr magneton, μ_N is the nuclear magneton, I is the moment of inertia, $L_x\hbar$ is the electronic angular momentum of the valence electrons about their respective nuclei along the axis of rotation, E_0 and E_n are the electronic energies in the ground and the excited states, and the prime on the summation sign indicates that $n\neq 0$.

The value of the high-frequency term may be determined by a straightforward calculation of Eq. (42). However, this calculation is very cumbersome if the excited state wave functions are known and impossible if they are not known. Several attempts have been made to estimate this term by simpler approximate methods.[10–12] In the next section we discuss Foley's method which is in closest agreement with the experimental results.

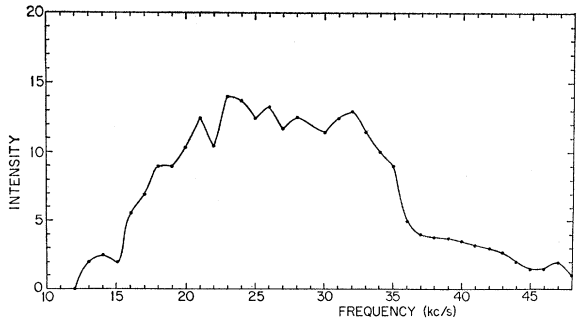

FIG. 3. Experimental KF resonance. $H\cong 800$ G, $(NI)_{\text{rf}}\cong 700$ ampere-turns, $T\cong 1030°$K.

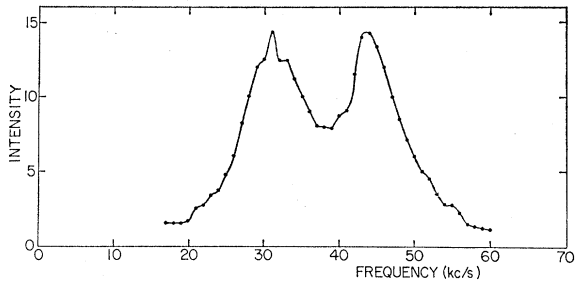

FIG. 4. Experimental CsF resonance. $H\cong 800$ G, $T\cong 913°$K.

White[10] suggests an evaluations of Eq. (42) from the measured value of the spin-rotational constant. This procedure, however, does not lead to good agreement with the experimental values.

2. Theoretical Evaluation of the High-Frequency Term

Foley[11] proposes the following method for the calculation of Eq. (42).

First, we observe that the measured values of the electric dipole moments of the alkali-halide molecules are lower than the product of their internuclear distances by the electronic charge. This indicates, according to Pauling, that there may be some contribution to the ground states of these molecules from neutral atoms.[13] A measure of this partially nonionic character is, therefore given by

$$\Gamma=1-\frac{\text{(electric dipole moment)}}{\text{(electron charge)}\times\text{(internuclear distance)}}. \tag{43}$$

Neglecting the contributions from the ionic fraction, the motion of the bonding p electron (the valence electron) of the halogen atom will account for the contribution to Eq. (42).

Following the pure precession hypothesis of Van Vleck,[14] we can think of the valence p electron as having a fixed angular momentum $\hbar$ precessing around the internuclear axis with zero projection on this axis for the ground state.

Using this approximation, we can calculate the matrix element $\langle p,\Pi|L_x|p,\Sigma\rangle$, which is the only nonvanishing

[9] G. C. Wick, Z. Physik **85**, 25 (1933); Nuovo Cimento **10**, 118 (1933).

[10] R. L. White, Rev. Mod. Phys. **27**, 276 (1955).
[11] H. M. Foley, Phys. Rev. **72**, 504 (1947).
[12] G. C. Wick, Phys. Rev. **73**, 51 (1948).
[13] L. Pauling, *Nature of the Chemical Bond* (Cornell University Press, Ithaca, New York, 1940).
[14] J. H. Van Vleck, Phys. Rev. **33**, 469 (1929).

TABLE IV. Comparison of Foley's electronic contribution with the experimental value (exp value of g_e = |ionic value of g_J − measured value of g_J|).

Molecule	Dipole moment (in Debye)		Γ	Dissociation energy (in Ergs)[g]	$g_{e,\text{Foley}}$	$g_{e,\text{exp}}$
LiF	6.28446	±0.00100[a]	0.163	$\leqslant 10.55\times10^{-12}$	$\geqslant 0.01497$	0.0165±0.0005
Li^7Cl	5.9	±1.3[b]	0.392	8.18	0.0244	0.0295±0.0032
Li^6Cl	5.9	±1.3[b]	0.392	8.18	0.0278	0.0339±0.0033
LiBr	6.19	±0.15[c]	0.407	7.22	0.0227	0.0392±0.0039
LiI	6.25	±0.20[c]	0.456	5.62	0.0261	0.0282±0.0089
NaI				5.07		0.0088±0.0047
KF	8.60	±0.09[d]	0.174	$\leqslant 9.47$	$\geqslant 0.00373$	0.0094±0.0012
RbF	8.80	±0.10[e]	0.189	8.66	0.00333	0.0032±0.0028
RbCl				$\geqslant 6.35$		0.0015±0.0018
CsF	7.875	±0.006[f]	0.300	8.98	0.00447	0.0170±0.0055
CsCl	10.42	0.02[f]	0.252	6.84	0.000193	0.0002±0.0011

[a] L. Wharton, W. Klemperer, L. P. Gold, R. Strauch, J. J. Gallagher, and V. E. Derr, J. Chem. Phys. **38**, 1203 (1963).
[b] D. T. F. Marple and J. W. Trischka, Phys. Rev. **103**, 597 (1956).
[c] A. Honig, M. Mandel, M. L. Stitch, and C. H. Townes, Phys. Rev. **96**, 629 (1954).
[d] G. W. Green and H. Lew, Can. J. Phys. **38**, 482 (1960).
[e] H. Lew, D. Morris, F. E. Geiger, and J. Eisinger, Can. J. Phys. **36**, 171 (1958).
[f] J. W. Trischka, J. Chem. Phys. **25**, 784 (1956).
[g] G. Herzberg, *Spectra of Diatomic Molecules* (D. Van Nostrand Company, Inc., Princeton, New Jersey, 1950).

matrix element involved in the sum of Eq. (42).

$$\langle p,\Pi|L_x|p,\Sigma\rangle=\tfrac{1}{2}\langle p,\Pi|L_+ + L_-|p,\Sigma\rangle$$
$$=\tfrac{1}{2}[(p-\Sigma)(p+\Sigma+1)]^{1/2}=1/\sqrt{2}.$$

Therefore,

$$|\langle\Pi|L_x|\Sigma\rangle|^2=\tfrac{1}{2}.$$

For the denominator $E_\Pi - E_\Sigma$ in Eq. (42), we can use a suitable average value, which will not be much larger than the excitation energy of the lowest Π-state.[12] The spectroscopic evidence indicates[15] that the energy curve as a function of the internuclear distance for the lowest excited Π state is almost horizontal for alkali halides. Therefore, the dissociation energy D_e can be used for $E_\Pi - E_\Sigma$.

Taking all these observations into account, Eq. (42) reduces to

$$g_{e,\text{Foley}}\cong 2.03\times10^{-51}\Gamma/I\times D_e,$$

where I is in g-cm² and D_e in ergs.

The dipole moment Γ, the dissociation energy $g_{e,\text{Foley}}$, and $g_{e,\text{exp}}$ are listed in Table IV.

The dipole moments of RbCl and NaI have not been measured. From the measured value of the rotational moment, using Foley's approximation, the dipole moments of RbCl and NaI can be calculated to be

$$\text{dipole moment of RbCl} \leq 11.4 \text{ Debye},$$
$$\text{dipole moment of NaI} \cong 6.2 \text{ Debye}.$$

TABLE V. Experimental and theoretical g_J-values.

Molecule	Ionic g_J	White's g_J	Foley's g_J	Experimental g_J	$g_{\text{Foley}}/g_{\text{exp}}$
LiF	0.0902	+0.0509	+0.0753	0.07367±0.00050	≤1.02
Li^7Cl	0.1143	+0.0942	+0.0899	0.0848 ±0.0032	1.06
Li^6Cl	0.1381	+0.1167	+0.1103	0.1042 ±0.0033	1.06
LiBr	0.1302		+0.1076	0.0911 ±0.0039	1.18
LiI	0.1350		+0.1089	0.1068 ±0.0089	1.02
NaI	0.0356			0.0268 ±0.0047	
KF	0.0270	−0.0392	−0.307	0.0364 ±0.0012	≥0.843
RbF	0.0409	−0.0534	−0.0442	0.0441 ±0.0028	1.00
RbCl	0.0171			0.0183 ±0.0018	
CsF	0.0451	−0.0606	−0.0496	0.0621 ±0.0055	0.80
CsCl	0.0211		−0.0213	0.0212 ±0.0011	1.00

In Table V the experimental total rotational g factor is compared with Foley, White, and ionic predictions.

Note that Foley's electronic correction is added to the total ionic value and not to $(1-\Gamma)$ times the ionic value. The latter alternative was tried and did not yield close agreement with the measured values.

3. Signs of the Rotational Moments

The ionic approximation, Eq. (41), gives the signs as well as the magnitudes of the rotational g factors. The electronic correction, being due to the rotation of negative charges, is always negative. In the theoretical determination carried out in the previous sections, both of these facts were taken into account. Since the calculated values are in close agreement with the experimental results, the correct signs should be those given by the ionic approximation.

4. The Fluorine Spin-Rotational Constant in CsF

A byproduct of these experiments was the unexpected appearance of the fluorine spin-rotational constant in the rotational spectrum of CsF. Figure 4 is the CsF rotational resonance. The difference of the two peaks gives the spin-rotational interaction of F. The value determined in this way would be quite accurate if the central minimum goes to zero. Otherwise, there would be a slight attraction of the two maxima toward each other by the contributions of the central portion. This causes an error of ±2.5 kc/sec, and the C_F value is

$$C_{F_{\text{in CsF}}}=13.5\pm2.5 \text{ kc/sec}.$$

[15] R. S. Mulliken, Phys. Rev. **51**, 310 (1937).